CHEMISTRY OF MATERIALS
Cite This: Chem. Mater. 2018, 30, 79−83
Communication
pubs.acs.org/cm

Colloidal CsX (X = Cl, Br, I) Nanocrystals and Their Transformation to $CsPbX_3$ Nanocrystals by Cation Exchange

Javad Shamsi,[†,‡] Zhiya Dang,[†] Palvasha Ijaz,[†,‡] Ahmed L. Abdelhady,[†,§] Giovanni Bertoni,[†] Iwan Moreels,[†] and Liberato Manna*[,†]

[†]Nanochemistry Department, Istituto Italiano di Tecnologia, Via Morego 30, 16163 Genova, Italy
[‡]Università degli Studi di Genova, Via Dodecaneso, 31, 16146 Genova, Italy
[§]Department of Chemistry, Faculty of Science, Mansoura University, Mansoura 35516, Egypt

Supporting Information

Cesium halides (CsX, X = Cl, Br, I) are interesting materials for studying the fundamental aspects of defects and doping, and for use in scintillation detectors, as is clear from the rich literature on thin films and bulk crystals of cesium halides over the past few decades.[1,2] In the 1960s, activated CsX crystals (with Tl, Na, and other elements) were introduced as γ-ray and charged particle detectors,[3] and several studies elucidated their band structures and the role of defects.[4,5] The interest in CsX was further triggered by the discovery of specific features in the optical spectra of doped CsX salts.[6,7] Also, the luminescence from nanosized aggregated $CsPbX_3$ phases was initially observed in CsX single crystal hosts in 1997,[8] which initiated additional investigations in the early 2000s.[9,10] Aceves et al.,[10] for example, found that Pb-doped CsBr bulk crystals have optical emission characteristics that are similar to those of Cs_4PbBr_6, $PbBr_2$, and $CsPbBr_3$ bulk crystals.[10] This indicates that Pb^{2+} ions, once inserted as substitutional dopants in the CsBr matrix, self-organize locally forming various binary and ternary Cs−Pb−Br structures.

This historical perspective suggests that CsX nanocrystals (NCs), and CsBr NCs in particular, are an interesting class of nanoparticles, and they can act as precursors for the synthesis of $CsPbX_3$ NCs, as we are reporting here. We were able to synthesize monodisperse colloidal CsX NCs with truncated octahedral shapes and simple cubic structure. The size of the CsX NCs could be tuned by varying the reaction temperature, in an ambient atmosphere. CsBr NCs were then reacted with lead oleate ($Pb(OA)_2$) to form core/shell CsBr/$CsPbBr_3$ NCs and finally $CsPbBr_3$ NCs by a partial $Cs^+ \rightarrow Pb^{2+}$ cation exchange. Although the reaction was accompanied by a noticeable shrinkage in the size of the NCs due to partial etching, there was a correlation between the initial size of the CsBr NCs and that of the $CsPbBr_3$ NCs. This means that, rather than undergoing a dissolution-recrystallization, the transformation undergoes a reorganization of the lattice following the insertion of Pb^{2+} ions and the ejection of Cs^+ ions. This is also supported by high resolution transmission electron microscopy (HRTEM) analysis, which indicated the formation of core/shell CsBr/$CsPbBr_3$ structures as intermediates. The emission from these core/shell structures in the early stages of the exchange was strongly blue-shifted from the corresponding bulk values of $CsPbBr_3$, as is expected from a shell thickness in the strong quantum confinement regime. This emission was, however, unstable and it red-shifted over time, even when the exchange was stopped by precipitating the particles and redispersing them in a clean solvent. This instability was also reflected in the aggregation of the purified particles, after overnight storage. The photoluminescence (PL) quantum yield (QY) of the fully transformed $CsPbBr_3$ NCs was stable and in the range of 32%−50%, which is, on average, lower than that of the corresponding particles that are prepared by the standard synthesis approach (which can be in the range of 50−90%). This is most likely due to the presence of structural and surface defects. Surface treatments with lead thiocyanate could increase the PLQY to 60%. Similarly, starting with CsCl NCs, $CsPbCl_3$ NCs could be synthesized, again with a correlation between the size of the starting CsCl NCs and that of the $CsPbCl_3$ NCs. In the case of the CsI → $CsPbI_3$ transformation, the control over the size of the final perovskite NCs was less accurate and resulted in polydisperse particles.

The CsX NCs were prepared by dissolving different types of salts as halide precursors, such as InX_3, ZnX_2, CoX_2, and tetrabutylammonium halide, in octadecene (ODE) together with oleylamine (OLA) and oleic acid (OA), then adding Cs-oleate (cesium carbonate dissolved in OA, CsOA) at different reaction temperatures, as is detailed in Table 1 and in the Supporting Information (SI). The reaction temperature and the specific halide precursors are the key parameters for producing uniform NCs as well as for having good control over the size. All NCs had truncated octahedra shapes, unless stated

Table 1. Reaction Conditions for the Synthesis of CsX NCs

CsX	Halide precursor	T (°C)	Size (nm)
CsCl	TBAC	90	PD[a] (cubes)
	$InCl_3$	90−130	20 ± 2−35 ± 3
CsBr	TBAB	90	PD (cubes + truncated octahedra)
	$ZnBr_2$	50−120	13 ± 1−30 ± 4
CsI	TBAI	90	PD (irregular shapes)
	ZnI_2	50−90	10 ± 1−22 ± 2

[a]PD: polydisperse.

Received: November 17, 2017
Revised: December 8, 2017
Published: December 11, 2017

DOI: 10.1021/acs.chemmater.7b04827
Chem. Mater. 2018, 30, 79−83

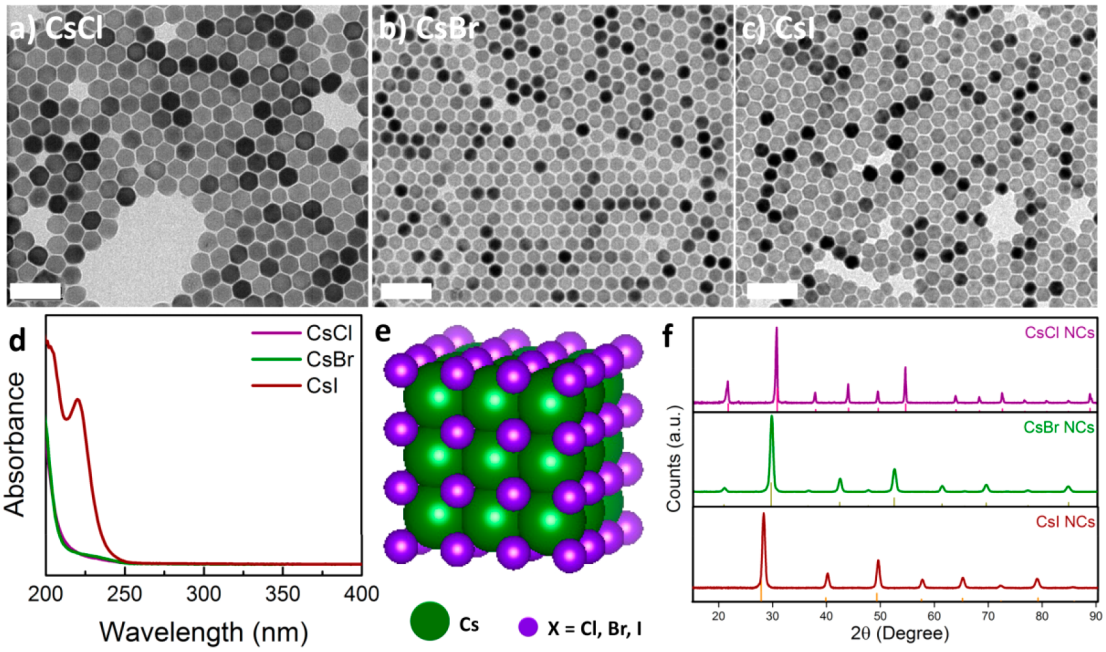

Figure 1. (a–c) Transmission electron microscopy (TEM) images of representative samples of CsX NCs. Scale bars are 100 nm in all images; (d) Optical absorption spectra of CsX NCs dispersed in hexane; (e) Sketch of the cubic structure of CsX; f) XRD patterns of the dried powders of CsX NCs, in comparison with the corresponding ICSD reference patterns (CsCl: 98-062-2366, CsBr: 98-002-2174, CsI: 98-004-4291).

otherwise. Conditions had to be adjusted for each halide composition, as is described below and is detailed in the SI.

CsCl. Initial tests using $CoCl_2$ led to deep blue tetragonal Cs_3CoCl_5 nanowires (Figure S1). Alternatively, dissolving $ZnCl_2$ salt in the same medium yielded orthorhombic Cs_2ZnCl_4 NCs (Figure S2). CsCl NCs could be grown using tetrabutylammonium chloride (TBAC), but they were nonuniform and polydisperse (Figure S3a). CsCl NCs with uniform shapes and tunable sizes (20–35 nm) could be finally synthesized using $InCl_3$ as a Cl precursor (Figures 1a and S3b). The results of these syntheses indicate that the size of the metal cation in the halide precursor dictates the type of Cl-based compounds that can be formed. Working with small cations leads to the formation of ternary compounds, such as Cs_3CoCl_5 and Cs_2ZnCl_4. Bigger cations, however, behave as spectator cations, which leads to the formation of CsCl NCs.

CsBr. The use of tetrabutylammonium bromide (TBAB) yielded NCs with broad size distributions (Figure S4b). CsBr NCs with uniform shapes and tunable sizes were prepared by using either $ZnBr_2$ or $CoBr_2$ as Br precursors (Figure 1b and Figure S4a). By employing ZnBr, the size of the CsBr NCs could be adjusted in the range of 13 to 30 nm by varying the reaction temperature (50–120 °C). However, reactions at 120 °C and above resulted in a broad size distribution (Figure S9b).

CsI. CsI NCs were prepared using ZnI_2 (Figure 1c). Similar to the other halides, tetrabutylammonium iodide could also be used as an iodide precursor, but this again yielded a polydisperse product (Figure S5a). Interestingly (and somewhat similar to the synthesis of the $CsPbX_3$ NCs[11]), the growth of CsI NCs was faster than that of Cl- or Br-based NCs at the same temperature. Therefore, to better control the size of the NCs, the syntheses were performed at a lower temperature range than that of the CsCl and CsBr cases (see SI and Table 1 for more details).

The absorption spectra of the CsX NCs are shown in Figure 1d. All these materials are essentially insulators and have large band gaps, therefore no band gap absorption should be observed down to 200 nm. Even for CsI, which has a 6.4 eV gap,[12] the onset should be at around 190 nm. The peak at ~220 nm for CsI (~5.6 eV) is most likely associated with the lowest energy state of the Γ(3/2, 1/2) exciton,[13,14] as is seen in bulk films of CsI. This exciton arises as a result of the transition from the Γ_{8^-} valence band states to the Γ_{6^+} conduction band states.[13,14] The reason that this state is located so far below (~0.8 eV) the conduction band minimum for CsI is because CsX has highly ionic lattices[15] with low dielectric constants, therefore excitons in these materials have large binding energies. The narrow absorption band at 220 nm is independent of the size of the CsI NCs (Figure S2b,c) and is comparable to that of bulk film.[13,14] This, again, is due to the strong exciton binding energy and consequent small exciton Bohr radius, hence a negligible quantum confinement effect would be seen in CsI. The absorption tails, which are in the region of 220–250 nm for CsBr and CsCl, are less understood, and might be due to deep trap states. The features around 200 nm are due to solvent absorption. X-ray diffraction (XRD) patterns of the dry powders of the as-prepared CsX NCs are in good agreement with the CsX simple cubic reference patterns, as shown in Figure 1e,f (both Cs^+ and X^- ions have 8-fold coordination in the simple cubic structure). The absence of any other impurity phase in the patterns proves that the cations that were introduced with the halide ions in the synthesis (e.g., Zn^{2+}, In^{3+}, etc.) do not form any crystalline compounds and are eliminated during the cleaning of the NCs.

The CsX NCs were then used as colloidal precursors to synthesize $CsPbX_3$ NCs. We focus most of our discussion on the transformation of CsBr to $CsPbBr_3$ NCs. Our first attempt was to react CsBr NCs with an excess amount of $PbBr_2$ (which was dissolved in a mixture of OLA, OA, and ODE) according to the following scheme:

$$CsBr + PbBr_2 \rightarrow CsPbBr_3 \quad (1)$$

DOI: 10.1021/acs.chemmater.7b04827
Chem. Mater. 2018, 30, 79–83

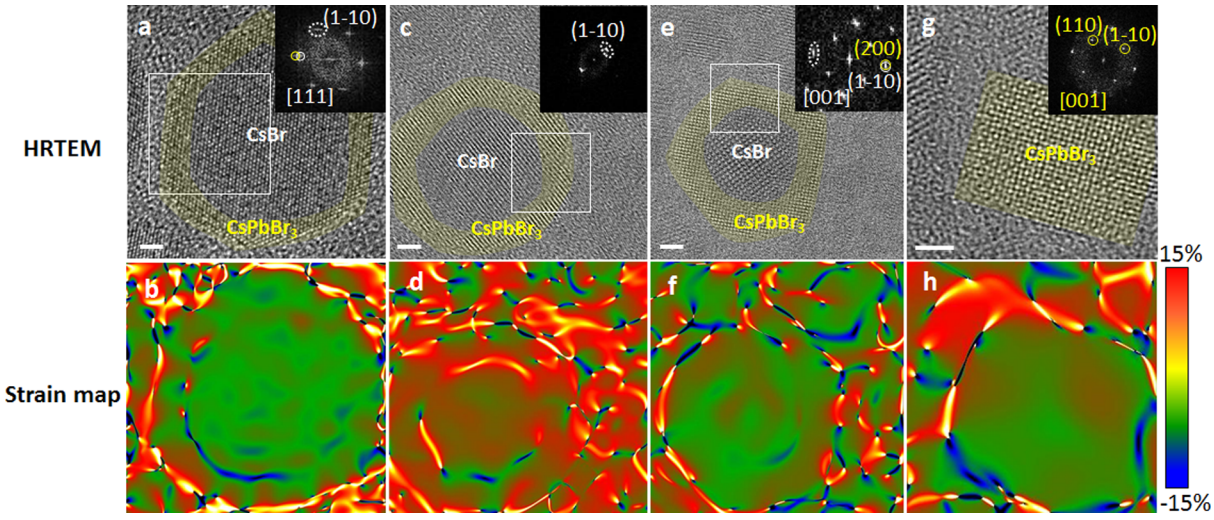

Figure 2. HRTEM images of NCs during different stages of the CsBr → $CsPbBr_3$ transformation (top) and corresponding strain maps (Δ_{xy}), obtained by geometric phase analysis (bottom). In the top panels, the perovskite domains are color coded in yellow. (Figure S10 of the SI shows a broader set of intermediate samples, without color coding). The scale bar is 2 nm; (a, b) a NC in is early stage, with a thin $CsPbBr_3$ shell; (c, d and e, f) Two NCs in their intermediate stages; (g, h) a fully transformed $CsPbBr_3$ NC. In panels a, c, and e, the inset is the FFT of the region that is delimited by the white box. The inset of panel g is the FFT of the whole image.

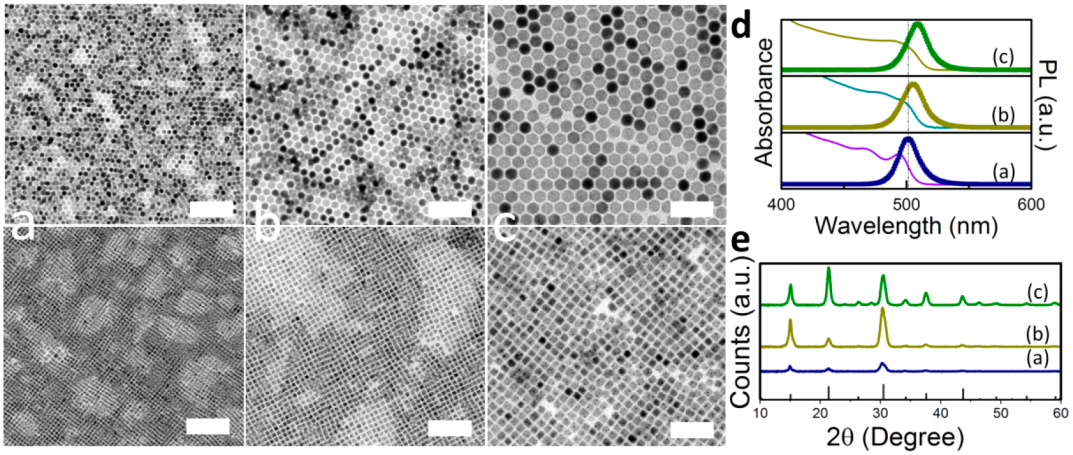

Figure 3. (a–c) TEM images of CsBr NCs of three representative sizes (top panels) and corresponding TEM images of the resulting $CsPbBr_3$ NCs (bottom panels). Scale bars correspond to 50 nm in all images; (d) corresponding optical spectra and (e) XRD patterns of the resulting $CsPbBr_3$ NCs (ICSD reference pattern: 98-009-7852).

These reactions were only partially successful. The reactivity of this system was low at room temperature, and resulted in mixtures of $CsPbBr_3$ nanocubes and partially transformed CsBr NCs with a double peak in PL (Figure S6) after an overnight reaction. Reactions at higher temperatures (70 °C) were poorly controllable: the size distribution of the $CsPbBr_3$ NCs was multimodal, as is evident from the multiple peaks in the PL spectrum (see Figure S7). Better control was possible by reacting the CsX NCs with Pb oleate ($Pb(OA)_2$, which was prepared by dissolving PbO in oleic acid), according to the following scheme:

$$3CsX + Pb(OA)_2 \rightarrow CsPbX_3 + 2CsOA \quad (2)$$

During preliminary tests, we employed small amounts of $Pb(OA)_2$ to investigate the initial stage of this reaction (see SI, experimental section). In this case, the solution turned fluorescent blue (with a peak at 468 nm and a PLQY of 22%), immediately after the addition. Such a blue PL was probably due to the formation of quantum confined $CsPbX_3$ domains on the surface of the CsBr NCs, whose shape remained essentially truncated octahedral at this stage (Figure S8a). The optical absorption and PL spectra of this sample red-shifted considerably over 1 day; the PL peak shifted from 468 to 486 nm (see Figure S8c,d for the corresponding PL decays) and the PLQY increased to 61%. This observation suggests the formation of bigger domains over time, even after a purification step (consisting of precipitating the particles and resuspending them in toluene). TEM analysis of a sample that was aged overnight after the purification step evidenced the strong aggregation of the NCs (Figure S8b). Reactions with larger amounts of $Pb(OA)_2$ yielded samples with a greener PL soon after the addition of the lead complex and were characterized by a variety of shapes (Figure S9), indicating a more advanced stage in the transformation. Finally, nearly monodisperse, pure $CsPbBr_3$ NCs could be prepared by adding an excess amount of $Pb(OA)_2$, as is detailed in the SI.

The samples at different stages of the transformation were characterized by the presence of an increasingly thicker

DOI: 10.1021/acs.chemmater.7b04827
Chem. Mater. 2018, 30, 79–83

perovskite shell on the CsBr NCs (Figure 2). Geometric phase analysis (GPA) was carried out on the HRTEM images of the NCs, which revealed a variation in the periodicities of the HRTEM contrast,[16] and strain at the interface of the core and shell regions. The initial CsBr NCs, as well as the samples in the early stages of the transformation, were often found oriented in the [111] zone axis, which is evidenced by a fast Fourier transform (FFT) showing six spots at equal angles (60°, Figure 2a). Even in the early stages of the transformation, the presence of $CsPbBr_3$ can be inferred by the elongated spots in the corresponding FFT images (which is highlighted by the white elliptical contour in the inset of Figure 2a) and by the presence of a strained interface separating the core and the shell. The orientational relationship between the CsBr core and the $CsPbBr_3$ shell in these early samples (Figure 2a–d) is CsBr [111] // $CsPbBr_3$ [001] and CsBr (1-10) // $CsPbBr_3$ (200). NCs with thicker $CsPbBr_3$ shells tended to be oriented in such a way that the CsBr lattice is in the [001] zone axis (Figure 2e,f). Notably, in samples with thicker $CsPbBr_3$ shells (Figure 2e, f), the orientational relationship between the core and the shell is different to that of thin shell samples, and is as follows: CsBr [001] // $CsPbBr_3$ [001], CsBr (1-10) // $CsPbBr_3$ (200) (see Figure S10 for more HRTEM images of the intermediate stages). Interestingly, this shape reduced the strain at the interface (see Figure 2f). The progressive transformation, namely the full conversion to $CsPbBr_3$ (Figure 2g,h) was indeed accompanied by a morphological change of the whole particle. The presence of the (Pb rich) perovskite shell in the intermediate samples was further confirmed by scanning TEM (STEM)-energy dispersive spectroscopy (EDS) analysis (see Figure S11): EDS evidenced a higher concentration of Pb in the outer regions of the NCs with respect to the central regions.[17]

CsBr NCs within a range of sizes (13–30 nm) could be fully transformed into $CsPbBr_3$ NCs (7–23 nm) at room temperature by adding an excess amount of $Pb(OA)_2$, as shown in Figure 3 for three different sizes of the starting CsBr NCs. In this case, not only did the NCs undergo a shape transformation (from truncated octahedral to cubic) but their overall size was also reduced. Although the transformation from CsBr to $CsPbBr_3$ entails the expulsion of two Cs^+ ions per every Pb^{2+} ion added, one should not expect such a large change in the volume of the particles, because the two materials have similar densities (4.44 g/cm^3 for CsBr and 4.75 g/cm^3 for $CsPbBr_3$).[18] The initial NCs therefore appeared to have undergone partial dissolution during the transformation, and this is understandable if one considers that the lattice needs to reorganize considerably when going from cubic CsBr (with both Cs^+ and Br^- ions in cubic coordination) to the perovskite structure. However, as can be seen from Figure 3, the size of the final $CsPbBr_3$ NCs is correlated to that of the initial CsBr NCs. This fact, and the evidence that $CsPbBr_3$ NCs were not observed growing separately from the CsBr NCs, while instead only intermediate core/shell structures were observed, excludes that the overall transformation goes through the dissolution of the CsBr NCs followed by the recrystallization of $CsPbBr_3$.

Optical data and XRD analyses further confirmed the full transformation of CsBr to $CsPbBr_3$, as shown in Figure 3d,e (additional two sizes of initial CsBr and final $CsPbBr_3$ NCs are shown in Figure S12). All data related to the transformation such as the size of the starting NCs as well as the transformed NCs and PL peak positions with full width at half-maxima are listed in Table S1. The relatively lower values of PLQY (ranging from 32% to 50%) of the $CsPbBr_3$ NCs prepared with our approach compared to those of the NCs prepared by direct synthesis[11] (50%–90%) demonstrate the formation of structural and surface defects acting as trap states during such a conversion. These are probably also the reason for the nonexponential PL decay of all samples (see SI, Figure S13). For the fitting, we required a sum of four exponentials (see SI, Table S1). We calculated the amplitude-averaged decay time, and found values of 3–5 ns for all $CsPbBr_3$ NCs except those with a 23 nm size, for which we obtained 17 ns. These values are generally in line with those of $CsPbBr_3$ NCs prepared by direct synthesis.[11]

Recently, Koscher et al. have reported a postsynthetic modification of $CsPbBr_3$ NCs in which adding a thiocyanate salt to the as-prepared perovskite NCs could effectively decrease the nonradiative exciton recombination.[19] We followed a modification of that protocol here, by adding a solution of $Pb(SCN)_2$ dissolved in OLA and OA and ODE to the NCs before the washing step. This treatment greatly improved the PLQY. As an example, in the case of the 16 nm $CsPbBr_3$ NCs the PLQY went from 38% to 60%. Adding a high excess of $Pb(SCN)_2$ solution did not raise the QY further. Although the overall increase was remarkable, the PLQY still did not reach the record values of the one-step grown $CsPbBr_3$ NCs, suggesting that our NCs have residual structural defects.[19] In addition, the lower PLQY of the bigger $CsPbBr_3$ NCs is a possible indication that structural defects were also present inside the NCs, and these are more likely to occur in bigger NCs.

CsCl and CsI NCs could also undergo the same type of transformation, delivering the corresponding perovskite NCs under the same reaction conditions. In the case of the CsCl NCs, there was a clear correlation between the size of the initial NCs and that of the corresponding perovskite NCs. For example, starting from two different sizes of CsCl NCs (20, 35 nm) we could prepare $CsPbCl_3$ NCs with average sizes of 15 and 29 nm, respectively. Figure S14 reports TEM images of the initial CsCl NCs, as well as optical, structural and morphological characteristics of the final $CsPbCl_3$ NCs. For CsI, the final $CsPbI_3$ NCs were considerably polydisperse (see Figure S15). In addition further investigation was in part compromised by the fast degradation of the final $CsPbI_3$ NCs.

Other Pb compounds were also tested to react with the CsX NCs in the attempt to transform them into $CsPbX_3$ NCs. We tested for example hexaphenyl lead (HPL, powder), which is easily soluble in toluene. This compound did not react with the CsX NCs at room temperature, as it required higher temperatures (100 °C or higher) to decompose and release Pb^{2+} ions. Unfortunately, under these conditions the CsX NCs were dissolved. A similar outcome was seen when employing $Pb(SCN)_2$, this time dissolved in a mixture of OLA, OA, and ODE. Like the $PbBr_2$ and HPL cases, this compound was not reactive enough toward the CsX NCs at room temperature.

In summary, we have reported a simple colloidal synthesis of CsX (X = Cl, Br, I) NCs with uniform shape and tunable size. Such NCs can then be used as colloidal precursors to synthesize $CsPbX_3$ NCs upon reaction with Pb^{2+} ions. A potential advantage of having monodisperse CsX NCs is that they should serve as precursors for other types of NCs including Cs^+ and halide ions in their composition, in addition to the halide perovskite NCs reported here.

DOI: 10.1021/acs.chemmater.7b04827
Chem. Mater. 2018, 30, 79–83

■ ASSOCIATED CONTENT

Supporting Information

The Supporting Information is available free of charge on the ACS Publications website at DOI: 10.1021/acs.chemmater.7b04827.

Experimental details of the syntheses of CsX NCs, their transformation to $CsPbX_3$, and related characterizations; TEM and optical characterization of CsX NCs prepared with various halide precursors; additional data on the transformation from CsBr to $CsPbBr_3$, also using different reaction routes; details on PL lifetime measurements; data on the CsCl → $CsPbCl_3$, and CsI → $CsPbI_3$ transformations (PDF)

■ AUTHOR INFORMATION

Corresponding Author

*L. Manna. E-mail: liberato.manna@iit.it.

ORCID

Javad Shamsi: 0000-0003-4684-5407
Ahmed L. Abdelhady: 0000-0002-6637-8853
Giovanni Bertoni: 0000-0001-6424-9102
Iwan Moreels: 0000-0003-3998-7618
Liberato Manna: 0000-0003-4386-7985

Notes

The authors declare no competing financial interest.

■ ACKNOWLEDGMENTS

The research leading to these results has received funding from the European Union seventh Framework Programme under Grant Agreement No. 614897 (ERC Consolidator Grant "TRANS-NANO").

■ REFERENCES

(1) Cardona, M.; Haensel, R.; Lynch, D. W.; Sonntag, B. Optical Properties of the Rubidium and Cesium Halides in the Extreme Ultraviolet. *Phys. Rev. B* **1970**, *2*, 1117−1131.

(2) Maldonado, J. R.; Coyle, S. T.; Shamoun, B.; Yu, M.; Gesley, M.; Pianetta, P. Cs Halide Photocathode for Multi-Electron-Beam Pattern Generator. *J. Vac. Sci. Technol., B: Microelectron. Process. Phenom.* **2004**, *22*, 3025.

(3) Nikl, M.; Yoshikawa, A. Recent R&D Trends in Inorganic Single-Crystal Scintillator Materials for Radiation Detection. *Adv. Opt. Mater.* **2015**, *3*, 463−481.

(4) Poole, R. T.; Jenkin, J. G.; Liesegang, J.; Leckey, R. C. G. Electronic Band Structure of the Alkali Halides. I. Experimental Parameters. *Phys. Rev. B* **1975**, *11*, 5179−5189.

(5) Halliday, M. T.; Hess, W. P.; Shluger, A. L. Structure and Properties of Electronic and Hole Centers in Csbr from Theoretical Calculations. *J. Phys.: Condens. Matter* **2015**, *27*, 245501.

(6) Prettl, W.; Siep, E. Low Lying Resonant Band Modes in Csbr and CsI Crystals Doped with In^+ and Tl^+. *Phys. Status Solidi B* **1971**, *44*, 759−767.

(7) Zhang, Z.; Zhao, Q.; Li, Y.; Ouyang, X. P. Electronic Structure and Optical Properties of CsI, CsI(Ag), and CsI(Tl). *J. Korean Phys. Soc.* **2016**, *68*, 1069−1074.

(8) Nikl, M.; Nitsch, K.; Polák, K.; Mihókova, E.; Zazubovich, S.; Pazzi, G. P.; Fabeni, P.; Salvini, L.; Aceves, R.; Barbosa-Flores, M.; et al. Quantum Size Effect in the Excitonic Luminescence of $CsPbX_3$-Like Quantum Dots in CsX (X = Cl, Br) Single Crystal Host. *J. Lumin.* **1997**, *72*, 377−379.

(9) Nikl, M.; Nitsch, K.; Mihokova, E.; Polak, K.; Fabeni, P.; Pazzi, G. P.; Gurioli, M.; Phani, R.; Santucci, S.; Scacco, A.; et al. Optical Properties of Pb^{2+}-Based Aggregated Phases in Csbr Thin Film and Single Crystal Matrices. *Radiat. Eff. Defects Solids* **1999**, *150*, 341−345.

(10) Aceves, R.; Babin, V.; Barboza Flores, M.; Fabeni, P.; Mihokova, E.; Nikl, M.; Nitsch, K.; Pazzi, G. P.; Perez Salas, R.; Zazubovich, N.; et al. Relaxed Excited States Origin and Structure in Lead-Doped Caesium Bromide. *Phys. Status Solidi B* **2001**, *223*, 745−756.

(11) Protesescu, L.; Yakunin, S.; Bodnarchuk, M. I.; Krieg, F.; Caputo, R.; Hendon, C. H.; Yang, R. X.; Walsh, A.; Kovalenko, M. V. Nanocrystals of Cesium Lead Halide Perovskites ($CsPbX_3$, X = Cl, Br, and I): Novel Optoelectronic Materials Showing Bright Emission with Wide Color Gamut. *Nano Lett.* **2015**, *15*, 3692−3696.

(12) Knittle, E.; Jeanloz, R. Structural and Bonding Changes in Cesium Iodide at High Pressures. *Science* **1984**, *223*, 53−56.

(13) Onodera, Y. Energy Bands in CsI. *J. Phys. Soc. Jpn.* **1968**, *25*, 469−480.

(14) Said, K. I.; Green, G. W. Optical Properties of Caesium Iodide in the Vacuum Ultraviolet. *J. Phys. C: Solid State Phys.* **1977**, *10*, 479.

(15) Dvorak, M.; Wei, S.-H.; Wu, Z. Origin of the Variation of Exciton Binding Energy in Semiconductors. *Phys. Rev. Lett.* **2013**, *110*, 016402.

(16) Hÿtch, M. J.; Snoeck, E.; Kilaas, R. Quantitative Measurement of Displacement and Strain Fields from Hrem Micrographs. *Ultramicroscopy* **1998**, *74*, 131−146.

(17) Dang, Z.; Shamsi, J.; Palazon, F.; Imran, M.; Akkerman, Q. A.; Park, S.; Bertoni, G.; Prato, M.; Brescia, R.; Manna, L. In Situ Transmission Electron Microscopy Study of Electron Beam-Induced Transformations in Colloidal Cesium Lead Halide Perovskite Nanocrystals. *ACS Nano* **2017**, *11*, 2124−2132.

(18) Samal, A. K.; Pradeep, T. Hybrid A-B-A Type Nanowires through Cation Exchange. *Nanoscale* **2011**, *3*, 4840−4847.

(19) Koscher, B. A.; Swabeck, J. K.; Bronstein, N. D.; Alivisatos, A. P. Essentially Trap-Free $CsPbBr_3$ Colloidal Nanocrystals by Postsynthetic Thiocyanate Surface Treatment. *J. Am. Chem. Soc.* **2017**, *139*, 6566−6569.

DOI: 10.1021/acs.chemmater.7b04827
Chem. Mater. 2018, 30, 79−83